

q deformed formulation of Hamiltonian SU(3) Yang-Mills theory

Tomoya Hayata,^{a,b} Yoshimasa Hidaka^{b,c,d,e,f}

^a*Departments of Physics, Keio University, 4-1-1 Hiyoshi, Kanagawa 223-8521, Japan*

^b*RIKEN iTHEMS, RIKEN, 2-1, Hirosawa, Wako, Saitama 351-0198, Japan*

^c*Theory Center, Institute of Particle and Nuclear Studies, High Energy Accelerator Research Organization (KEK), 1-1 Oho, Tsukuba 305-0801, Japan*

^d*Graduate Institute for Advanced Studies, SOKENDAI, 1-1 Oho, Tsukuba 305-0801, Japan*

^e*nternational Center for Quantum-field Measurement Systems for Studies of the Universe and Particles (QUP), KEK, 1-1 Oho, Tsukuba 305-0801, Japan*

^f*Department of Physics, Faculty of Science, University of Tokyo, 7-3-1 Hongo Bunkyo-ku Tokyo 113-0033, Japan*

E-mail: hayata@keio.jp, hidaka@post.kek.jp

ABSTRACT: We study SU(3) Yang-Mills theory in $(2 + 1)$ dimensions based on networks of Wilson lines. With the help of the q deformation, networks respect the (discretized) SU(3) gauge symmetry as a quantum group, i.e., $SU(3)_k$, and may enable implementations of SU(3) Yang-Mills theory in quantum and classical algorithms by referring to those of the stringnet model. As a demonstration, we perform a mean-field computation of the groundstate of $SU(3)_k$ Yang-Mills theory, which is in good agreement with the conventional Monte Carlo simulation by taking sufficiently large k . The variational ansatz of the mean-field computation can be represented by the tensor networks called infinite projected entangled pair states. The success of the mean-field computation indicates that the essential features of Yang-Mills theory are well described by tensor networks, so that they may be useful in numerical simulations of Yang-Mills theory.

Contents

1	Introduction	1
2	Networks and algebras	2
2.1	Algebraic data	2
2.2	$SU(3)_k$ quantum group	6
3	$SU(3)_k$ Yang Mills theory on a square lattice	7
4	Computational methods	10
4.1	Expectation values of observables	10
4.2	Minimization of \mathcal{H}	15
5	Numerical results	15
6	Discussion	19
	Bibliography	21

1 Introduction

Quantum chromodynamics (QCD) is a nonabelian gauge theory describing the strong interaction between quarks mediated by gluons [1]. One of the most important properties of QCD is the so-called asymptotic freedom: The interaction between quarks and gluons becomes weak and the perturbative computations work remarkably well at short distance such as deep inelastic scattering, while it becomes strong at long distance leading to the confinement of quarks and gluons inside hadrons. To understand the physics of confinement and describe hadrons from QCD, we need to deal with QCD nonperturbatively. To this end, lattice QCD has been developed, which provides us the most established and powerful computational methods of quantum field theories based on Monte Carlo techniques. However, some problems remain unsolved such as the QCD phase diagram or equation of state at low temperature and high density, and real-time dynamics of QCD [2-5]. In those problems, the importance sampling breaks down due to the complex measure of path integrals, which is the notorious sign problem.

Inspired by the recent developments in quantum technology- and information-based tools such as quantum simulation [6, 7] and tensor networks [8, 9] in condensed matter systems, much efforts have been devoted to exploring the potential of those tools in high-energy physics [10, 11]. Indeed, those tools were found to be effective, e.g., in studying nonequilibrium dynamics of lattice gauge theories in $(1 + 1)$ dimensions [12, 13]. However, we face

many challenges in applications to higher dimensions since we need to tackle with the complex dynamics of gauge fields [14]. Even if we limit ourselves to pure Yang-Mills theories, i.e., nonabelian gauge theories without quarks for simplifying the problem as is commonly done in theoretical studies of QCD, implementation of gauge fields on quantum simulators or tensor networks is still a nontrivial task: We need to approximate infinite-dimensional Hilbert space of gauge fields as finite degrees of freedom with keeping gauge invariance manifestly. Although it is not fully established yet, there is some progress in SU(2) [15–26]. However, only a little is known about SU(3) [27–29] although it is preliminary to quantum or classical simulation of QCD.

In this paper, we formulate a regularized Kogut-Susskind Hamiltonian [30] of SU(3) lattice Yang-Mills theory in (2+1) dimensions based on networks of Wilson lines, which are known as spin networks for SU(2) [31–35], by generalizing the formulation described in refs. [19, 24, 25]. To approximate continuous space of SU(3) as finite degrees of freedom, we deform SU(3) group into SU(3)_k quantum group, and construct the Kogut-Susskind Hamiltonian of SU(3)_k Yang-Mills theory. As its first application, we perform the mean-field computation of the groundstate. We study the k dependence of observables to estimate k required for discussing the physics in the $k \rightarrow \infty$ limit.

The remainder of this paper is organized as follows. We review algebras of networks and the q deformation in section 2. The crucial difference between SU(2), and SU(3) or SU(N) [$N > 2$] is multiplicity of representations, which is elaborated in section 2. Then, using algebras of networks, we construct the Kogut-Susskind Hamiltonian of SU(3)_k Yang-Mills theory on a square lattice in section 3. We give technical details of the mean-field computation, particularly the computation of expectation values based on graphs in section 4. Numerical results are shown in section 5. We compare the mean-field computation of SU(3)_k Yang-Mills theory with the Monte Carlo simulation of SU(3) Yang-Mills theory. Finally, we briefly discuss future improvements of this work in section 6.

2 Networks and algebras

2.1 Algebraic data

The gauge invariant physical Hilbert space of a lattice gauge theory can be represented using a basis that corresponds to a network of Wilson lines. In the case of SU(2), such a network is known as a spin network [31–35]. If the gauge group is continuous, the Hilbert space of gauge fields exhibits infinite degrees of freedom even on a finite lattice, and it is necessary to approximate the Hilbert space as finite degrees of freedom for quantum simulations. We regularize the theory by deforming the SU(3) group into the SU(3)_k quantum group. The original SU(3) group is recovered by the $k \rightarrow \infty$ limit. The algebra generated by the network of Wilson lines of the quantum group is described by the unitary modular tensor category (UMTC), which is employed as an anyon model [36]. In this section, we briefly summarize the algebra of networks necessary for Hamiltonian formalism, following the conventions in ref. [37]. For more comprehensive details, see, e.g., references [36, 38].

Wilson lines are labeled by the representations of the gauge group, and we represent them by a, b, c, \dots . For $SU(2)_k$ gauge theory, these representations are equivalent to the angular momentum j . In $SU(N)_k$, they correspond to the highest weight vectors or the so-called Dynkin labels. For a given representation a , there exists an anti-representation, which we write as \bar{a} . They are graphically represented by directed lines:

$$\begin{array}{c} | \\ \uparrow \\ a \end{array} = \begin{array}{c} | \\ \downarrow \\ \bar{a} \end{array} . \quad (2.1)$$

Wilson lines can be composed. The product of Wilson lines is decomposed into irreducible representations. This decomposition is represented by the fusion rule:

$$a \times b = \sum_c N_{ab}^c c, \quad (2.2)$$

which satisfies the associativity,

$$\sum_e N_{ab}^e N_{ec}^d = \sum_f N_{af}^d N_{bc}^f, \quad (2.3)$$

and $N_{ab}^c = N_{ba}^c = N_{bc}^{\bar{a}} = N_{\bar{a}b}^c$. N_{ab}^c is the multiplicity of the composition of representations, which is a nonnegative integer. For example, in $SU(3)$ group, the product of the adjoint representation $\mathbf{8}$, $\mathbf{8} \otimes \mathbf{8}$, is decomposed into $\mathbf{1} \oplus \mathbf{8} \oplus \mathbf{8} \oplus \overline{\mathbf{10}} \oplus \mathbf{10} \oplus \mathbf{27}$, which implies $N_{\mathbf{8}\mathbf{8}}^{\mathbf{1}} = N_{\mathbf{8}\mathbf{8}}^{\mathbf{10}} = N_{\mathbf{8}\mathbf{8}}^{\overline{\mathbf{10}}} = N_{\mathbf{8}\mathbf{8}}^{\mathbf{27}} = 1$ and $N_{\mathbf{8}\mathbf{8}}^{\mathbf{8}} = 2$. Here, we have used the dimension of the representations as a label of representations. If we use Dynkin labels (p, q) , the correspondences are $\mathbf{1} = (0, 0)$, $\mathbf{8} = (1, 1)$, $\mathbf{10} = (2, 0)$, $\overline{\mathbf{10}} = (0, 2)$, and $\mathbf{27} = (2, 2)$.

When \mathbf{N}_a is regarded as a matrix whose matrix components are given by $[\mathbf{N}_a]_b^c = N_{ab}^c$, the largest eigenvalue of \mathbf{N}_a is called the quantum dimension d_a , which is generically not integers. From $N_{ab}^c = N_{\bar{a}b}^c$, the quantum dimension of the anti-representation \bar{a} is equal to that of the representation a , i.e., $d_{\bar{a}} = d_a$. At $k \rightarrow \infty$, they are reduced to the dimensions of the ordinary representation matrices, e.g., $d_{(1,0)} = d_{(0,1)} = 3$, $d_{(1,1)} = 8$, etc. The complete expression for $SU(3)_k$ is shown in section 2.2.

A network of Wilson lines may have a junction, which is labeled by an additional quantum number μ to distinguish states with multiplicity when $N_{ab}^c \geq 2$:

$$\begin{array}{c} a \quad b \\ \searrow \quad \swarrow \\ \mu \\ \uparrow \\ c \end{array} , \quad \begin{array}{c} c \\ \uparrow \\ \mu \\ \swarrow \quad \searrow \\ a \quad b \end{array} , \quad (2.4)$$

where the vertex label runs $\mu \in \{1, 2, \dots, N_{ab}^c\}$. Each junction must satisfy $N_{ab}^c > 0$.

To construct the algebra of a network of Wilson lines, we need information about the local composition, decomposition, and fusion transformations of Wilson lines at junctions. This

information can be specifically derived from the composition and decomposition of representations of (quantum) groups. This algebra characterizes the algebra of anyons in a topological phase and possesses a topological nature, implying that the anyons or equivalently Wilson lines can be freely deformed as long as they do not intersect in spacetime. The graphical representation of the topological deformation rules can be summarized as follows:

$$\begin{array}{c} \begin{array}{c} c' \\ \uparrow \mu' \\ \circlearrowleft \\ \downarrow \mu \\ c \end{array} \end{array} = \delta_c^{c'} \delta_\mu^{\mu'} \sqrt{\frac{d_a d_b}{d_c}} \begin{array}{c} \uparrow \\ c \end{array} , \quad (2.5)$$

$$\begin{array}{c} \begin{array}{c} a \\ \uparrow \\ \parallel \\ \uparrow \\ b \end{array} \end{array} = \sum_{c,\mu} \sqrt{\frac{d_c}{d_a d_b}} \begin{array}{c} \begin{array}{c} a \quad b \\ \searrow \quad \swarrow \\ \uparrow \mu \\ \swarrow \quad \searrow \\ a \quad b \end{array} \end{array} , \quad (2.6)$$

$$\begin{array}{c} \begin{array}{c} a \quad b \quad c \\ \searrow \quad \swarrow \quad \nearrow \\ \mu \quad e \quad \nu \\ \downarrow \\ d \end{array} \end{array} = \sum_{f,\rho,\sigma} [F_d^{abc}]_{(e,\mu,\nu)(f,\rho,\sigma)} \begin{array}{c} \begin{array}{c} a \quad b \quad c \\ \searrow \quad \swarrow \quad \nearrow \\ \sigma \quad f \quad \rho \\ \downarrow \\ d \end{array} \end{array} . \quad (2.7)$$

Here, $[F_d^{abc}]_{(e,\mu,\nu)(f,\rho,\sigma)}$ are called the F -symbols. They are unitary matrices, i.e.,

$$[(F_d^{abc})^{-1}]_{(e,\mu,\nu)(f,\rho,\sigma)} = [(F_d^{abc})^\dagger]_{(e,\mu,\nu)(f,\rho,\sigma)} = [F_d^{abc}]_{(f,\rho,\sigma)(e,\mu,\nu)}^* , \quad (2.8)$$

and satisfy the pentagon equation

$$\begin{aligned} & \sum_{\delta} [F_e^{fcd}]_{(g,\beta,\gamma)(l,\nu,\delta)} [F_e^{abl}]_{(f,\alpha,\delta)(k,\mu,\lambda)} \\ &= \sum_{h,\sigma,\psi,\rho} [F_g^{abc}]_{(f,\alpha,\beta)(h,\psi,\sigma)} [F_e^{ahd}]_{(g,\sigma,\gamma)(k,\rho,\lambda)} [F_k^{bcd}]_{(h,\psi,\rho)(l,\nu,\mu)} . \end{aligned} \quad (2.9)$$

In the UMTC, there is also a braiding exchange represented by

$$\begin{array}{c} \begin{array}{c} a \quad b \\ \searrow \quad \swarrow \\ \mu \\ \downarrow \\ c \end{array} \end{array} = \sum_{\nu} [R_c^{ab}]_{\mu\nu} \begin{array}{c} \begin{array}{c} a \quad b \\ \searrow \quad \swarrow \\ \nu \\ \downarrow \\ c \end{array} \end{array} , \quad (2.10)$$

which is not used in our paper. $[R_c^{ab}]_{\mu\nu}$ must be compatible to the F -symbols, and the compatibility condition is described by Hexagon equations.

Let us use the deformation rules to derive some relations. A Wilson loop with represen-

tation a is graphically represented as

$$\text{tr } U_a = a \left[\text{circle with a central dot and an arrow pointing clockwise} \right]. \quad (2.11)$$

Here, we introduced a defect at the center of the loop to prevent it from collapsing when contracted. When the defect is absent, it reduces to

$$a \left[\text{circle with an arrow pointing clockwise} \right] = d_a, \quad (2.12)$$

by choosing $b = \bar{a}$ and $c = 0$ in eq. (2.5). Two Wilson loops with representations a and b can be deformed using eqs (2.5) and (2.6) to

$$\begin{aligned} a \left[\text{circle with a central dot and an arrow pointing clockwise} \right] &= \sum_{\mu, c} \frac{\sqrt{d_c}}{\sqrt{d_a d_b}} c \left[\text{circle with a central dot, an arrow pointing clockwise, and a loop labeled } \mu \text{ around it} \right] \\ &= \sum_{\mu, c} \frac{\sqrt{d_c}}{\sqrt{d_a d_b}} c \left[\text{circle with a central dot, an arrow pointing clockwise, and a loop labeled } \mu \text{ around it} \right] \\ &= \sum_{c, \mu} \frac{\sqrt{d_c}}{\sqrt{d_a d_b}} \frac{\sqrt{d_{\bar{b}} d_{\bar{a}}}}{\sqrt{d_{\bar{c}}}} c \left[\text{circle with a central dot and an arrow pointing clockwise} \right] \\ &= \sum_c N_{ab}^c c \left[\text{circle with a central dot and an arrow pointing clockwise} \right]. \end{aligned} \quad (2.13)$$

In the last equality, we used $d_{\bar{a}} = d_a$, etc. This leads to the fusion rule of Wilson loops:

$$\text{tr } U_a \text{tr } U_b = \sum_c N_{ab}^c \text{tr } U_c. \quad (2.14)$$

Furthermore, using eq. (2.12), we obtain

$$d_a d_b = \sum_c N_{ab}^c d_c. \quad (2.15)$$

Let us derive the inverse relation of eq. (2.15). Noting $d_{\bar{b}} = d_b$, $d_{\bar{c}} = d_c$, and $N_{ab}^{\bar{c}} = N_{ac}^b$, we obtain

$$d_a d_b = \sum_c N_{ac}^b d_c. \quad (2.16)$$

Multiplying both sides by d_a and summing over a yield the inverse relation of eq. (2.15),

$$\mathcal{D}^2 d_b = \sum_{a, c} N_{ac}^b d_a d_c. \quad (2.17)$$

where \mathcal{D} is the total quantum dimension defined by

$$\mathcal{D} := \sqrt{\sum_a d_a^2}. \quad (2.18)$$

In a gauge theory, of course, the Wilson lines are generally not topological. However, as will be seen later, these rules play a crucial role in computing the action of the operators on a physical state.

2.2 $SU(3)_k$ quantum group

We are interested in $SU(3)_k$ in our numerical calculations; let us summarize the mathematical objects used in section 4 such as the fusion multiplicities, second order Casimir invariants, and quantum dimensions for $SU(3)_k$. For $SU(3)_k$, an irreducible representation is represented by Dynkin labels, $a = (p_a, q_a)$, where p_a and q_a are the number of single and double box columns in the Young tableaux, respectively.

The fusion multiplicities are given as [39]

$$N_{ab}^c = (k_0^{\max} - k_0^{\min} + 1)\delta_{ab}^c, \quad (2.19)$$

where

$$k_0^{\min} = \max(p_a + q_a, p_b + q_b, p_c + q_c, \mathcal{A} - \min(p_a, p_b, q_c), \mathcal{B} - \min(q_a, q_b, p_c)), \quad (2.20)$$

$$k_0^{\max} = \min(\mathcal{A}, \mathcal{B}), \quad (2.21)$$

$$\mathcal{A} = \frac{1}{3}(2(p_a + p_b + q_c) + q_a + q_b + p_c), \quad (2.22)$$

$$\mathcal{B} = \frac{1}{3}(p_a + p_b + q_c + 2(q_a + q_b + p_c)), \quad (2.23)$$

$$\delta_{ab}^c = \begin{cases} 1 & \text{if } k_0^{\max} > k_0^{\min} \text{ and } \mathcal{A}, \mathcal{B} \in \mathbb{Z}_+ \\ 0 & \text{otherwise} \end{cases}. \quad (2.24)$$

Here, \mathbb{Z}_+ represents the set of non-negative integers.

Using the q -deformation parameter,

$$q = \exp\left(i \frac{2\pi}{k+3}\right), \quad (2.25)$$

the so-called q -number is defined as

$$[n] := \frac{q^{\frac{n}{2}} - q^{-\frac{n}{2}}}{q^{\frac{1}{2}} - q^{-\frac{1}{2}}} = \frac{\sin\left(\frac{\pi}{k+3}n\right)}{\sin\left(\frac{\pi}{k+3}\right)}. \quad (2.26)$$

Note that the q -deformation parameter ‘ q ’ is different from q in the Dynkin labels (p, q) . In

the following, q appears only as the Dynkin labels, so there will be no confusion.

The second order Casimir invariant $C_2(a)$ is given as [40]¹.

$$C_2(a) = \frac{1}{2} \left(\left[\frac{p_a}{3} - \frac{q_a}{3} \right]^2 + \left[\frac{2p_a}{3} + \frac{q_a}{3} + 1 \right]^2 + \left[\frac{p_a}{3} + \frac{2q_a}{3} + 1 \right]^2 - 2 \right). \quad (2.27)$$

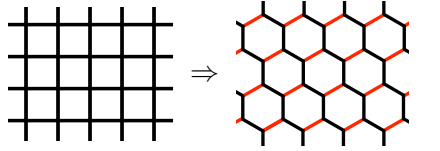
Similarly, the quantum dimension is given by [41]

$$d_a = \frac{1}{[2]} [p_a + 1][q_a + 1][p_a + q_a + 2]. \quad (2.28)$$

To the best of our knowledge, the general compact form of the F -symbols is not known for $SU(3)_k$. Some special cases for a small k were studied in ref. [42]. As discussed in section 4, the method we use does not require a specific form of the F -symbols.

3 $SU(3)_k$ Yang Mills theory on a square lattice

We consider $SU(3)_k$ Yang Mills theory on a square lattice in $(2 + 1)$ dimensions. Square lattices with four-point vertices are not represented in the algebra of the previous section. In order to treat them, we deform the square lattice into a honeycomb lattice with three-point vertices by inserting auxiliary edges [25]:



The diagram shows a square lattice on the left, which is transformed into a honeycomb lattice on the right. The honeycomb lattice consists of black lines forming a hexagonal pattern. Red lines are added to the honeycomb lattice, connecting the midpoints of opposite edges of each hexagon, effectively creating a square lattice structure within the honeycomb lattice. The transformation is indicated by a right-pointing arrow.

$$, \quad (3.1)$$

where the red lines represent the auxiliary edges. Note that this deformation is equivalent to the original square lattice as long as no electric field operator acts on the auxiliary edges.

This deformation (3.1) allows the physical state on the lattice to be represented using Wilson-line networks in the previous section. A basis of the physical Hilbert space is labeled by the representation and multiplicity on edges and vertices, respectively:

$$|\mathbf{a}; \boldsymbol{\mu}\rangle = \prod_{e \in \mathcal{E}} |a_e\rangle \prod_{v \in \mathcal{V}} |\mu_v\rangle, \quad (3.2)$$

which satisfies the orthogonal relation:

$$\langle \mathbf{a}'; \boldsymbol{\mu}' | \mathbf{a}; \boldsymbol{\mu} \rangle = \delta_{\mathbf{a}', \mathbf{a}} \delta_{\boldsymbol{\mu}', \boldsymbol{\mu}} = \prod_{e \in \mathcal{E}} \delta_{a'_e, a_e} \prod_{v \in \mathcal{V}} \delta_{\mu'_v, \mu_v}. \quad (3.3)$$

Here, \mathcal{E} and \mathcal{V} are the set of edges and vertices. Note that the incoming a , b , and outgoing c edges connected to a vertex cannot be arbitrary and must satisfy $N_{ab}^c > 0$. The state $|\mathbf{a}; \boldsymbol{\mu}\rangle$ is

¹We choose that the normalization factor of $C_2(a)$ is half of the value used in ref. [40].

generated by applying a network of Wilson line operators to $|\mathbf{0}; \mathbf{0}\rangle$. A state around a plaquette is graphically represented by

$$\prod_{i=1}^6 |a_i\rangle |c_i\rangle |\mu_i\rangle = \begin{array}{c} \begin{array}{c} c_4 \\ \downarrow \\ \begin{array}{c} a_4 \quad \mu_4 \quad a_3 \\ \swarrow \quad \downarrow \quad \searrow \\ \mu_5 \quad \mu_3 \\ \swarrow \quad \downarrow \quad \searrow \\ a_5 \quad \mu_6 \quad a_2 \\ \swarrow \quad \downarrow \quad \searrow \\ c_6 \quad a_6 \quad \mu_1 \quad a_1 \\ \downarrow \\ c_1 \end{array} \\ \end{array} \end{array} . \quad (3.4)$$

The Kogut-Susskind Hamiltonian of $SU(3)_k$ Yang-Mills theory has the form,

$$H = \frac{1}{2} \sum_{e \in \tilde{\mathcal{E}}} E_i^2(e) - \frac{K}{2} \sum_{f \in \mathcal{F}} (\text{tr } U_{(1,0)}(f) + \text{tr } U_{(0,1)}(f)). \quad (3.5)$$

Here, $\tilde{\mathcal{E}} \subset \mathcal{E}$ is the set of blacked edges in eq. (3.1), and \mathcal{F} is the set of hexagonal plaquettes in eq. (3.1). $E_i(e)$ is the electric field, i.e., generator of $SU(3)_k$, and $\text{tr } U_{(1,0)}(f)$ is the Wilson loop that circles the edges of the plaquette f clockwise. Note that the coupling strength K and conventional coupling constant g can be related as $K = 1/g^4$ in the lattice unit.

Let us consider the action of the Hamiltonian on a state. The action of the electric field term in the Hamiltonian, i.e., E_i^2 term, is graphically represented as

$$E_i^2 \begin{array}{c} \uparrow \\ | \\ a \\ | \\ \downarrow \end{array} = C_2(a) \begin{array}{c} \uparrow \\ | \\ a \\ | \\ \downarrow \end{array} . \quad (3.6)$$

Here, $C_2(a)$ is the second order Casimir invariant given in Eq. (2.27)². On the other hand, the action of a Wilson loop $\text{tr } U_d$ with $d = (1, 0)$ or $(0, 1)$ is given as [43]

$$\text{tr } U_d \begin{array}{c} \begin{array}{c} c_4 \\ \downarrow \\ \begin{array}{c} a_4 \quad \mu_4 \quad a_3 \\ \swarrow \quad \downarrow \quad \searrow \\ \mu_5 \quad \mu_3 \\ \swarrow \quad \downarrow \quad \searrow \\ a_5 \quad \mu_6 \quad a_2 \\ \swarrow \quad \downarrow \quad \searrow \\ c_6 \quad a_6 \quad \mu_1 \quad a_1 \\ \downarrow \\ c_1 \end{array} \\ \end{array} = \sum_{\{a'_i, \mu'_i\}} \prod_{i=1}^6 [F_{a'_i}^{c_i a_{i-1} d}]_{(a_i, \mu_i, \mu_{i+1}), (a'_{i-1}, \mu'_{i-1}, \mu'_i)} \begin{array}{c} \begin{array}{c} c_4 \\ \downarrow \\ \begin{array}{c} a'_4 \quad \mu'_4 \quad a'_3 \\ \swarrow \quad \downarrow \quad \searrow \\ \mu'_5 \quad \mu'_3 \\ \swarrow \quad \downarrow \quad \searrow \\ a'_5 \quad \mu'_6 \quad a'_2 \\ \swarrow \quad \downarrow \quad \searrow \\ c_6 \quad a'_6 \quad \mu'_1 \quad a'_1 \\ \downarrow \\ c_1 \end{array} \\ \end{array} \end{array} , \quad (3.7)$$

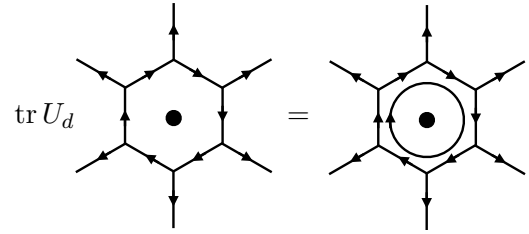
where $a'_0 = a'_6$, $\mu_0 = \mu_6$, $\mu'_0 = \mu'_6$, and $\mu'_7 = \mu'_1$. We note that eq. (3.7) works for any representation. Equation (3.7) can be graphically derived by using the topological deformation rules discussed in the previous section. First, let us put defects in the center of all plaquettes.

²There may be a choice of the action of the electric fields. We employ the q -deformed Casimir invariant to ensure consistency with the quantum group structure. On the other hand, a previous study uses the Casimir invariant without the q deformation [24].

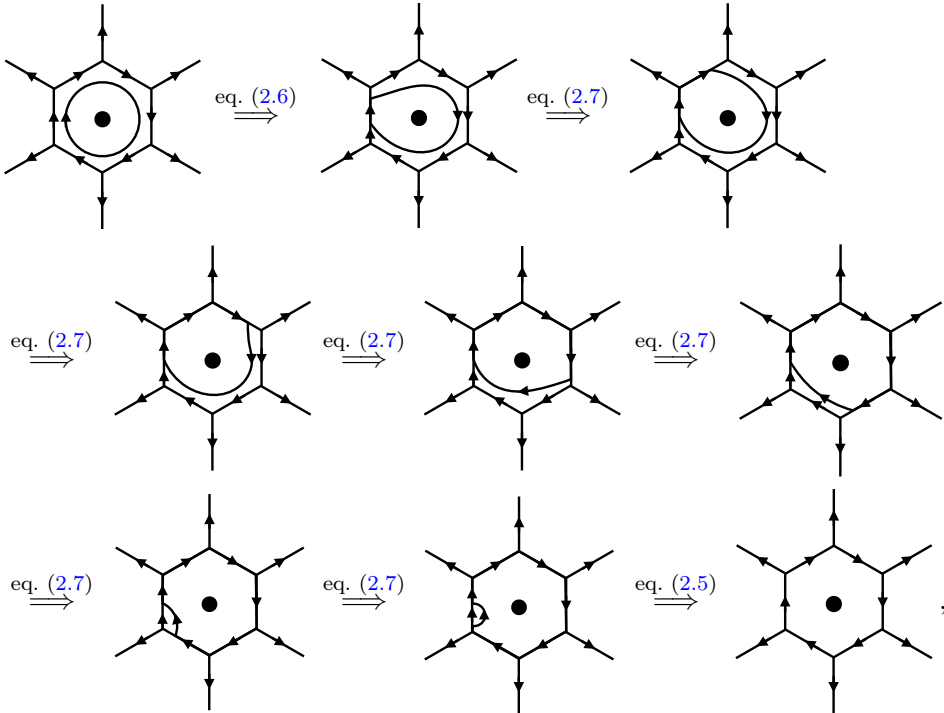
For a plaquette, it is graphically represented as


(3.8)

Here, the indices have been dropped for brevity. The defect is responsible for making the network non-trivial in its topological deformation. The action of $\text{tr} U_d$ on a plaquette is expressed by a loop encircling the defect,


(3.9)

Using the deformation rules in eqs (2.5)-(2.7):


(3.10)

we obtain eq. (3.7), by tracing the changes of indices.

4 Computational methods

We employ a variational ansatz introduced in refs. [24, 44],

$$|\Psi\rangle = \prod_{f \in \mathcal{F}} \sum_{a_f} \psi(a_f) \text{tr} U_{a_f}(f) |\Psi_0\rangle, \quad (4.1)$$

where $|\Psi_0\rangle = |\mathbf{0}; \mathbf{0}\rangle$, and variational parameters $\psi(a)$ are normalized as $\sum_a |\psi(a)|^2 = 1$ such that $\langle \Psi | \Psi \rangle = 1$. We impose open boundary conditions and take the infinite volume limit. Assuming the translational invariance of the groundstate, we employ the same wave function for all plaquettes. In the following subsections, we explain how we compute the expectation value of an operator in $|\Psi\rangle$ using graph rules introduced in the previous sections, and how we solve the variational problem.

4.1 Expectation values of observables

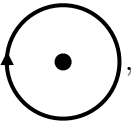
Let us evaluate the expectation value of an operator $\langle O \rangle := \langle \Psi | O | \Psi \rangle$. As an example, we consider the expectation value of a Wilson loop, $O = \text{tr} U_d(\partial S)$, where ∂S represents the path of the Wilson loop, which is the boundary of an area S . The expectation value is given as

$$\begin{aligned} & \langle \text{tr} U_d(\partial S) \rangle \\ &= \langle \Psi_0 | \text{tr} U_d(\partial S) \left(\prod_{f \in \mathcal{F}} \sum_{a_f, b_f} \psi^*(a_f) \psi(b_f) \text{tr} U_{\bar{a}_f}(f) \text{tr} U_{b_f}(f) \right) | \Psi_0 \rangle \\ &= \sum_{\{a\}, \{b\}, \{c\}} \left(\prod_{f' \in \mathcal{F}} \psi^*(a_{f'}) \psi(b_{f'}) N_{\bar{a}_{f'}, b_{f'}}^{c_{f'}} \right) \langle \Psi_0 | \text{tr} U_d(\partial S) \prod_{f \in \mathcal{F}} \text{tr} U_{c_f}(f) | \Psi_0 \rangle, \end{aligned} \quad (4.2)$$

where we introduce a shorthand notation,

$$\sum_{\{a\}} = \prod_{f \in \mathcal{F}} \sum_{a_f}. \quad (4.3)$$

We repeatedly used the fact that all Wilson loops commute with each other. We also used

$$\text{tr} U_{b_f}(f) |\Psi_0\rangle = b_f \left(\bigcirc \right), \quad (4.4)$$


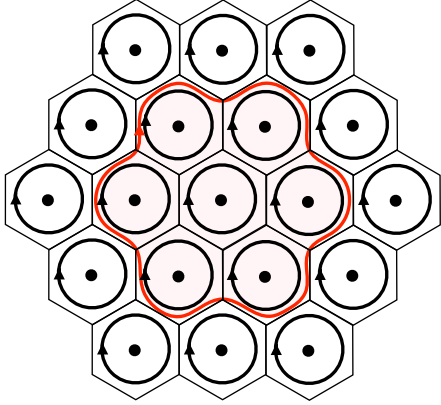
and the fusion rule of the Wilson loops in eqs. (2.13) and (2.14) on the same plaquette to obtain the second line. The nontrivial part of the calculation is now the evaluation of

$$\langle \Psi_0 | \text{tr} U_d(\partial S) \prod_{f \in \mathcal{F}} \text{tr} U_{c_f}(f) | \Psi_0 \rangle. \quad (4.5)$$

To this end, let us consider the state

$$\text{tr } U_d(\partial S) \prod_{f \in \mathcal{F}} \text{tr } U_{c_f}(f) |\Psi_0\rangle, \quad (4.6)$$

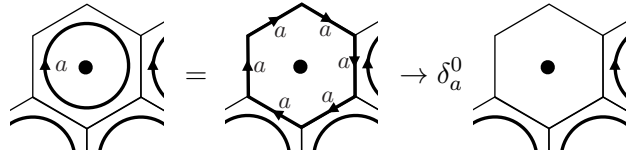
and then apply $\langle \Psi_0 |$ on the state. We consider a small lattice with boundaries for illustrating the computation, and the state (4.6) is represented as

$$U_d(\partial S) \prod_{f \in \mathcal{F}} \text{tr } U_{c_f}(f) |\Psi_0\rangle = \text{Diagram}, \quad (4.7)$$


where the red line is the path of ∂S , and the inside region shaded by light gray is S . By acting $\langle \Psi_0 |$ on the state, we evaluate the expectation value. Let us first look at the boundary. A given boundary plaquette can be deformed as

$$\text{Diagram} = \text{Diagram}, \quad (4.8)$$


When we compute the partial inner product with $\langle \Psi_0 |$ for three edges on the boundary in eq. (4.8), only states with trivial representation survive, since $\langle 0|a\rangle = \delta_a^0$. Thus, we can replace the plaquette operator by

$$\text{Diagram} = \text{Diagram} \rightarrow \delta_a^0 \text{Diagram}. \quad (4.9)$$


The contribution of this plaquette to the expectation value (4.2) becomes trivial:

$$\sum_{a,b,c} \psi^*(a)\psi(b)N_{ab}^c\delta_c^0 = \sum_{a,b} \psi^*(a)\psi(b)\delta_b^a = 1, \quad (4.10)$$

where we employ $N_{ab}^0 = \delta_b^a$. Repeating this procedure until we reach ∂S , eq. (4.7) becomes

$$(4.11)$$

Where the Wilson loops overlap, we can use eq. (2.6) to evaluate

$$(4.12)$$

Here we used the same reduction as eq. (4.9). Repeating this procedure until the red line shrinks to a point, we obtain

$$(4.13)$$

$$= d_d \left(\prod_{f \in S} \frac{\delta_{c_i}^d}{d_d} \right)$$

By plugging the obtained numerical factor into eq. (4.2), the expectation value of the Wilson loop is (see also ref. [45])

$$\begin{aligned}
\langle \text{tr } U_d(\partial S) \rangle &= d_d \prod_{f \in S} \sum_{a_f, b_f, c_f} \psi^*(a_f) \psi(b_f) N_{a_f b_f}^{c_f} \frac{\delta_{c_f}^{\bar{d}}}{d_d} \\
&= d_d \left(\frac{\sum_{a,b} N_{ab}^a \psi^*(a) \psi(b)}{d_d} \right)^{|S|} \\
&= d_d \exp(-|S| \sigma_d),
\end{aligned} \tag{4.14}$$

where we employ $N_{ab}^{\bar{d}} = N_{db}^a$ in the second line, $|S|$ represents the number of the hexagonal plaquettes inside the path ∂S , and σ_d is the string tension,

$$\sigma_d := \ln \frac{d_d}{\sum_{a,b} N_{ab}^a \psi^*(a) \psi(b)}. \tag{4.15}$$

If σ_d is of order unity, the Wilson loop exhibits the area law. As is seen later, the wave function in the string net condensed state is $\psi(a) = d_a / \mathcal{D}$ [43]. From eq. (2.17), we find that the string tension σ_d vanishes, or equivalently, the expectation value of the Wilson loop in eq. (4.2) becomes the unity.

Next, we compute the expectation value of the Hamiltonian (3.5). Using eq. (4.14), the expectation value of the Wilson loop on the hexagonal plaquette with the representation (1, 0) is evaluated as

$$\langle \Psi | \text{tr } U_{(1,0)}(f) | \Psi \rangle = \sum_{a,b} M_{ab} \psi^*(a) \psi(b), \tag{4.16}$$

where we write $M_{ab} = N_{(1,0)b}^a$. Using the same method to that of the expectation value of the Wilson loop, we can evaluate $\langle E_i^2(e) \rangle$:

$$\langle E_i^2(e) \rangle = \sum_{a,b,a',b'} \psi^*(a') \psi^*(b') \psi(a) \psi(b) \langle \Psi_0 | \text{tr } U_{\bar{a}'}(f) \text{tr } U_{\bar{b}'}(f') E_i^2(e) \text{tr } U_a(f) \text{tr } U_b(f') | \Psi_0 \rangle. \tag{4.17}$$

Here, f and f' are the plaquettes adjoining the edge e . The contribution from a plaquette not adjacent to the edge e becomes trivial, as does in the computation of the expectation value of the Wilson loop. Therefore, it is sufficient to consider the adjacent hexagonal plaquettes. We use the same technique as before. First, we apply E_i^2 to the state

$$\text{tr } U_a(f) \text{tr } U_b(f') | \Psi_0 \rangle = \begin{array}{c} \text{Diagram of two adjacent hexagonal plaquettes. The left hexagon has a central dot and a counter-clockwise arrow labeled 'a'. The right hexagon has a central dot and a counter-clockwise arrow labeled 'b'. The two hexagons share a vertical edge. } \end{array} \tag{4.18}$$

as

$$\begin{aligned}
E_i^2(e) \text{ (two hexagons with loops } a \text{ and } b) &= \sum_{c,\mu} \frac{\sqrt{d_c}}{\sqrt{d_a d_b}} E_i^2(e) \text{ (two hexagons with loops } a, c, b \text{ and } \mu) \\
&= \sum_{c,\mu} \frac{\sqrt{d_c}}{\sqrt{d_a d_b}} C_2(c) \text{ (two hexagons with loops } a, c, b \text{ and } \mu) .
\end{aligned} \tag{4.19}$$

In the first and second lines, we used eqs. (2.6) and (3.6), respectively. Next, we apply the Wilson loop to the state

$$\begin{aligned}
&\text{tr } U_{\bar{a}'}(f) \text{tr } U_{\bar{b}'}(f') E_i^2(e) \text{tr } U_a(f) \text{tr } U_b(f') |\Psi_0\rangle \\
&= \sum_{c,\mu} \frac{\sqrt{d_c}}{\sqrt{d_a d_b}} C_2(c) \text{ (two hexagons with loops } a, a', c, b, b') \\
&\rightarrow \sum_{c,\mu} \frac{\sqrt{d_c}}{\sqrt{d_a d_b}} C_2(c) \frac{\delta_a^{a'} \delta_b^{b'}}{d_a d_b} \text{ (two hexagons with loops } a, c, b) \\
&= \sum_c N_{\bar{a}b}^c \frac{\sqrt{d_c}}{\sqrt{d_a d_b}} C_2(c) \frac{\delta_a^{a'} \delta_b^{b'}}{d_a d_b} \frac{\sqrt{d_a d_c}}{\sqrt{d_b}} d_b \text{ (two hexagons)} \\
&= \sum_c N_{\bar{a}b}^c C_2(c) \frac{d_c}{d_a d_b} \delta_a^{a'} \delta_b^{b'} \text{ (two hexagons)} ,
\end{aligned} \tag{4.20}$$

where we used eq. (4.12) twice to reduce the second line to the third line, eqs. (2.5) and (2.12) to reduce the third line to the fourth line, and $d_a = d_{\bar{a}}$ to reduce the fourth line to the fifth line. Therefore the expectation value of $E_i^2(e)$ is given as

$$\langle E_i^2(e) \rangle = \sum_{a,b,c} C_2(c) N_{\bar{a}b}^c \frac{d_c}{d_a d_b} |\psi(a)|^2 |\psi(b)|^2. \tag{4.21}$$

Finally, let us compute the expectation value of the Hamiltonian. Using eqs (4.16) and (4.21),

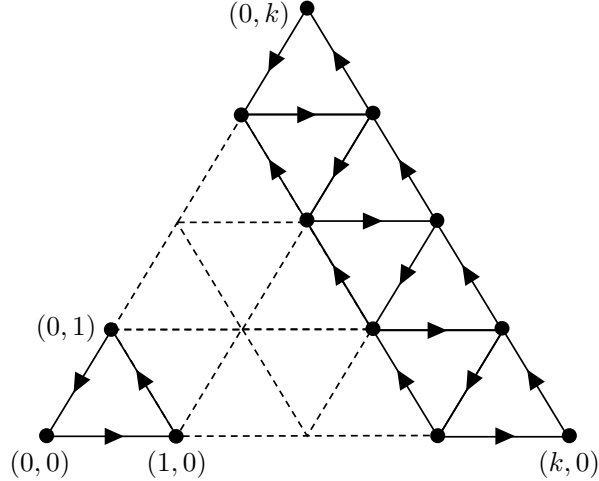


Figure 1. Diagram for $SU(3)_k$. Arrows indicate the action of the fundamental Wilson loop.

the Hamiltonian density reads

$$\begin{aligned} \mathcal{H} &= \frac{1}{V} \langle H \rangle \\ &= \sum_{a,b,c} C_2(c) N_{ab}^c \frac{d_c}{d_a d_b} |\psi(a)|^2 |\psi(b)|^2 - \frac{K}{2} \sum_{a,b} \psi^*(a) \left(M_{ab} + M_{ab}^\dagger \right) \psi(b), \end{aligned} \quad (4.22)$$

where V is the number of the plaquettes, and M_{ab} is the adjacency matrix, which is one between representations connected by arrows in figure 1 otherwise 0. Note that since each plaquette has four E_i^2 terms, and a E_i^2 term (an edge) is shared by two plaquettes, the factor of the E_i^2 term in eq. (4.22) is $4 \times 1/2 \times 1/2 = 1$.

4.2 Minimization of \mathcal{H}

To minimize \mathcal{H} with the constraint $\sum_a |\psi(a)|^2 = 1$, we solve the imaginary-time evolution

$$\begin{aligned} \partial_\tau \psi(\tau, a) &= - \sum_{b,c} \left(C_2(c) N_{ab}^c \frac{d_c}{d_a d_b} |\psi(\tau, b)|^2 \psi(\tau, a) + C_2(c) N_{ba}^c \frac{d_c}{d_a d_b} |\psi(\tau, b)|^2 \right) \\ &\quad + \frac{K}{2} \sum_{a,b} \left(M_{ab} + M_{ab}^\dagger \right) \psi(\tau, b) - \Lambda \left(\sum_b |\psi(\tau, b)|^2 - 1 \right) \psi(\tau, a), \end{aligned} \quad (4.23)$$

where the last term is a penalty term to impose $\sum_b |\psi(b)|^2 = 1$.

5 Numerical results

We solved eq. (4.23) using the fourth-order Runge-Kutta method. The initial state is $\psi(0, a) = \delta_{a,(0,0)}$, and we used $\psi(50, a)$ as the groundstate wavefunction. We take $\Lambda = 400 \max(K, 1)$,

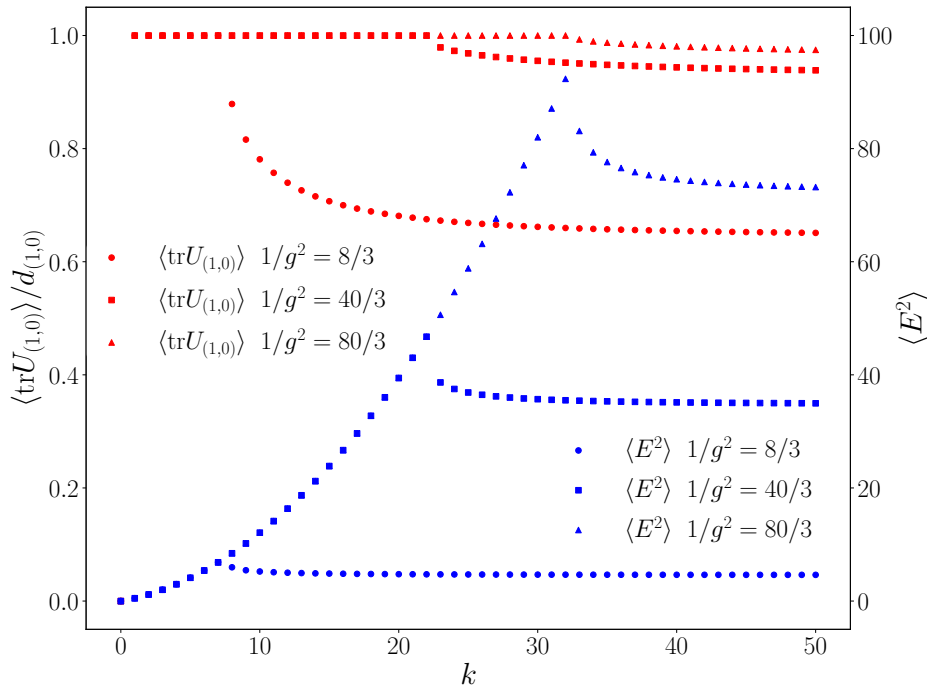


Figure 2. k dependence of the electric and magnetic Hamiltonian density $\langle E_i^2 \rangle$ and $\langle \text{tr} U_{(1,0)} \rangle$ with the lattice coupling $1/g^2 = 8/3, 40/3, \text{ and } 80/3$.

and the time step of the Runge-Kutta method $\delta\tau$ is fixed with $\delta\tau = 0.25/\Lambda$. First, we show the k dependence of the electric and magnetic Hamiltonian density, $\langle E_i^2 \rangle$ and $\langle \text{tr} U_{(1,0)} \rangle$ with changing $1/g^2$ from small to large in figure 2. As is clearly seen in the k dependence of $\langle E_i^2 \rangle$, we see the convergence of observables as k increases, and larger k is needed for simulating the groundstate with larger $1/g^2$. Note that the groundstate is in the topological phase below a critical k , where the Wilson loop is topological, i.e., $\langle \text{tr} U_a \rangle = d_a$ as in eq. (2.12). We find that a moderate coupling $1/g^2 \sim 1$ requires $k \sim 10$ from figure 2. This may be reachable in the near future qudit computers [24, 46], where the basis of a single link or multiplicity is encoded into a single qudit. Importantly, the convergence accompanies a phase transition. This phase transition is interesting in views of quantum information or condensed matter physics but it is unwanted for simulation of high-energy physics. As detailed below, $SU(3)_k$ Yang-Mills theory with small k is not smoothly connected to $SU(3)$ Yang-Mills theory of our target, and thus we should take great care of the k dependence of observables when available k is limited.

To study the phase transition and phase structure more quantitatively, we fix k and study the $1/g^2$ dependence of observables. We find that the phase transition occurs as continuously changing $1/g^2$ from small to large between the confined and topological phases (see figure 4 for $k = 10$ and 20). We compute the critical $1/g^2$ as a function of k , and draw the phase diagram in figure 3. We fitted the data by $k = a(1/g^2 - 1/g_0^2)^b$, and obtained $a = 5.58(3)$, $b = 0.543(1)$,

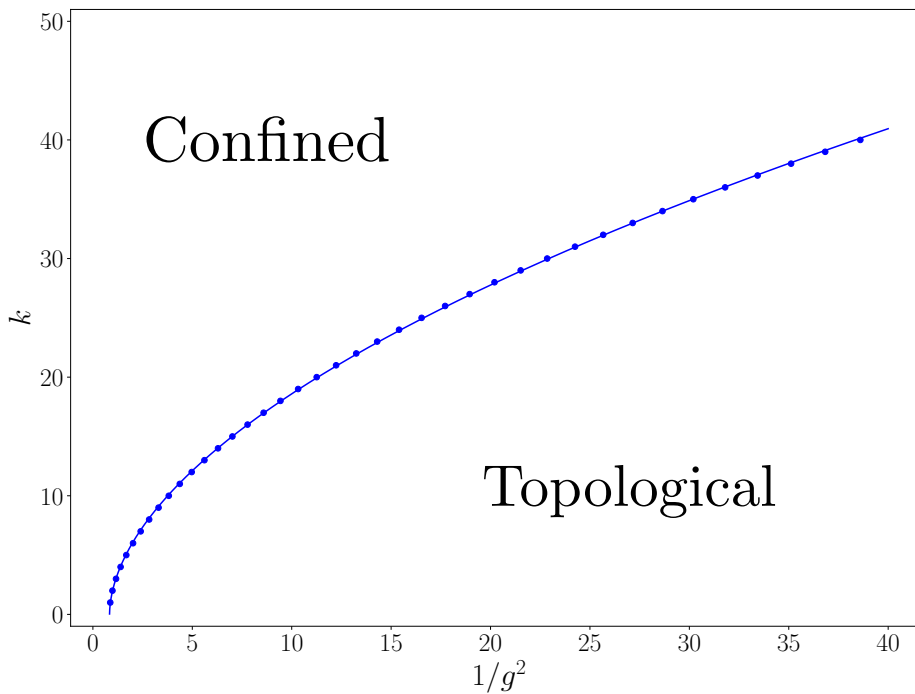


Figure 3. Phase structure of $SU(3)_k$ Yang-Mills theory. The blue dot represents the critical coupling at each k . We fitted the data by $k = a(1/g^2 - 1/g_0^2)^b$, which is shown by the blue curve. The confined phase is smoothly connected to $SU(3)$ Yang-Mills theory. The topological phase exhibits topological order described by the string-net condensation. The phase transition occurs between these phases when crossing the curve.

and $1/g_0^2 = 0.838(5)$. The fitting curve is also shown in figure 3. It would be useful for estimating k , which is required for simulating the continuum limit. Now, let us elaborate on the phase structure. The confined phase is smoothly connected to the vacuum at $1/g^2 = 0$, i.e., the groundstate in the strong coupling limit, while the topological phase is smoothly connected to the groundstate in the weak coupling limit. Within the mean field computation, the groundstate of the topological phase is the same as that of the string-net model [24, 43], i.e., the string-net condensed state $|\Psi_{\text{string-net}}\rangle = \prod_{f \in \mathcal{F}} U_{\text{reg}}(f)|0\rangle/\mathcal{D}^2$, where $U_{\text{reg}}(f)$ is the Wilson loop of the regular representation, and given explicitly as $U_{\text{reg}}(f) = \sum_a d_a U_a(f)$, and \mathcal{D} is the total quantum dimension. The string-net condensed state exhibits topological order, which is classified by the UMTC. In short, to simulate $SU(3)$ Yang-Mills theory, which is necessary for high-energy physics, we should keep k , so that the state is in the confined phase (an extrapolation to the $k \rightarrow \infty$ limit is also needed), while the state should be in the topological phase to use topological quantum computation or quantum error correcting code [47, 48].

To give a more quantitative discussion on the physics in the $k \rightarrow \infty$ limit, we compare the mean field computation of $SU(3)_k$ Yang-Mills theory with the conventional Monte Carlo

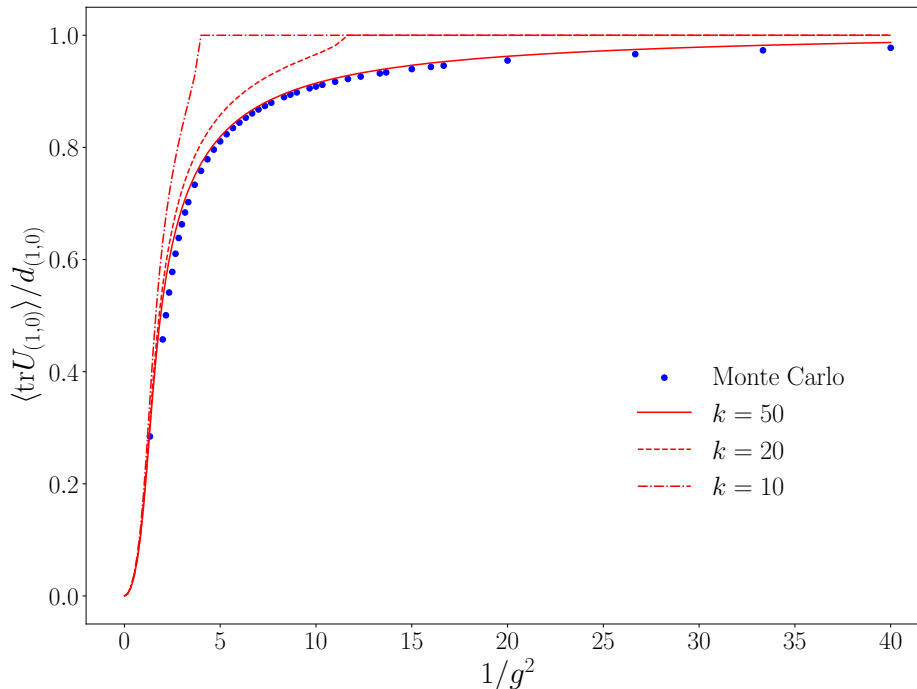


Figure 4. $1/g^2$ dependence of the fundamental Wilson loop on the minimum plaquette. Mean field computation of $SU(3)_k$ Yang-Mills theory (red curves) is compared with the Monte Carlo simulation of continuous $SU(3)$ Yang-Mills theory (blue dots). Monte Carlo data is taken from ref. [49].

simulation of $SU(3)$ Yang-Mills theory. We show the expectation value of the fundamental Wilson loop on the hexagonal plaquette in figure 4, where the Monte Carlo data are taken from ref. [49]. Using sufficiently large k , our mean field computation is in good agreement with the Monte Carlo data. This means that the variational ansatz (4.1) captures the essential features of Yang-Mills theory. Note that the number of variational parameters N_v is scaled as $N_v = k^2/2 + 3k/2 + 1$, and e.g., $N_v = 1326$ when $k = 50$. Furthermore, using eq. (4.15), we can compute the string tension of the Wilson loop of any representation. We show the string tension of the fundamental Wilson loop in figure 5. In this case, we see the quantitative difference between the mean-field and Monte Carlo results even if we use a large k . This may be the fault of the mean-field computation, in which the large Wilson loop is given by the product of the small uncorrelated Wilson loops as described in section 4. It may be rather surprising that such a simple computation leads to quantitative results. We can generalize the variational ansatz by following refs. [50, 51], which may capture correlations missed in the present ansatz and enable the more correct description of Yang-Mills theory. Such a generalization may also be important to obtain finite-size corrections to the area law in eq. (4.15). Finally, we show the string tension of the Wilson loop of all representations as a function of the second order Casimir invariant with changing $1/g^2$ in figure 6, and with changing k in figure 7. It

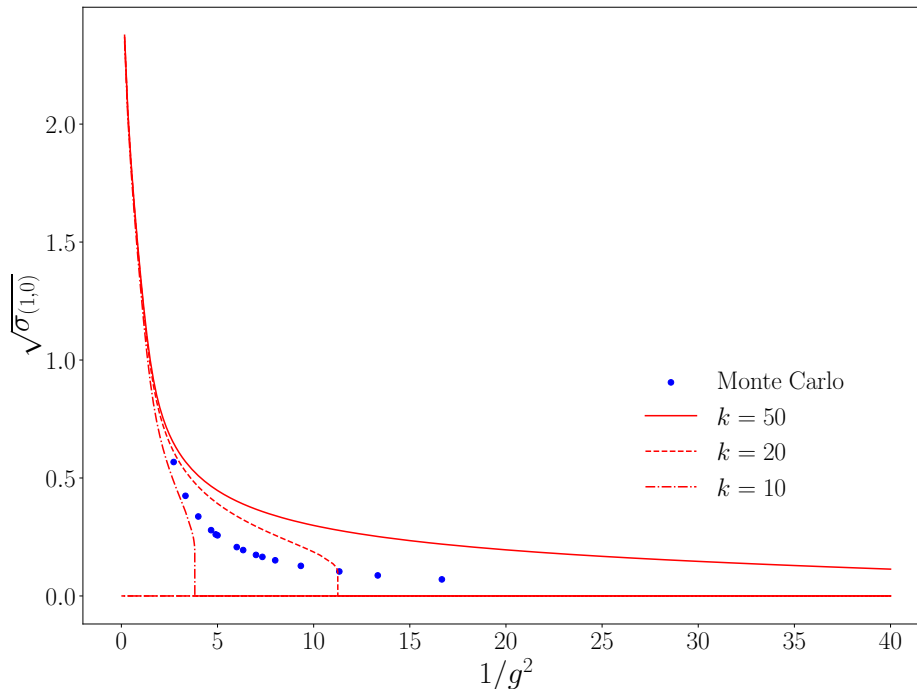


Figure 5. $1/g^2$ dependence of the string tension of the fundamental Wilson loop. The mean field computation of $SU(3)_k$ Yang-Mills theory (red curves) is compared with the Monte Carlo simulation of $SU(3)$ Yang-Mills theory (blue dots). Monte Carlo data is taken from ref. [49]. We used the lattice unit.

is known that the string tension of the Wilson loop of representation a is proportional to the second order Casimir invariant of the representation $C_2(a)$, i.e., $\sigma_a = \kappa C_2(a)$, which is referred to as the Casimir scaling in the literature [52–55]. From figures 6, and 7, we see that the Casimir scaling holds in the region far from the strong coupling limit, but is still in the confined phase in figure 3. This is natural because the Casimir scaling does not hold in the strong and weak coupling limits with finite k . In the strong coupling limit, the wave function is $\psi(a) = \delta_a^0$, so that the string tension diverges for all representations. On the other hand in the topological phase, the Wilson loop is always unity, which means the string tension is zero for all representations.

6 Discussion

We have generalized the formulation of a regularized Hamiltonian for $SU(2)$ lattice Yang-Mills theory based on the spin network and q deformation to $SU(3)$. As a demonstration, we have performed the mean-field computation, which shows good agreements with the Monte Carlo simulation. The variational ansatz (4.1) is known to be represented by the tensor network called infinite projected entangled pair states (iPEPS) [24, 44, 56–58]. The success of the

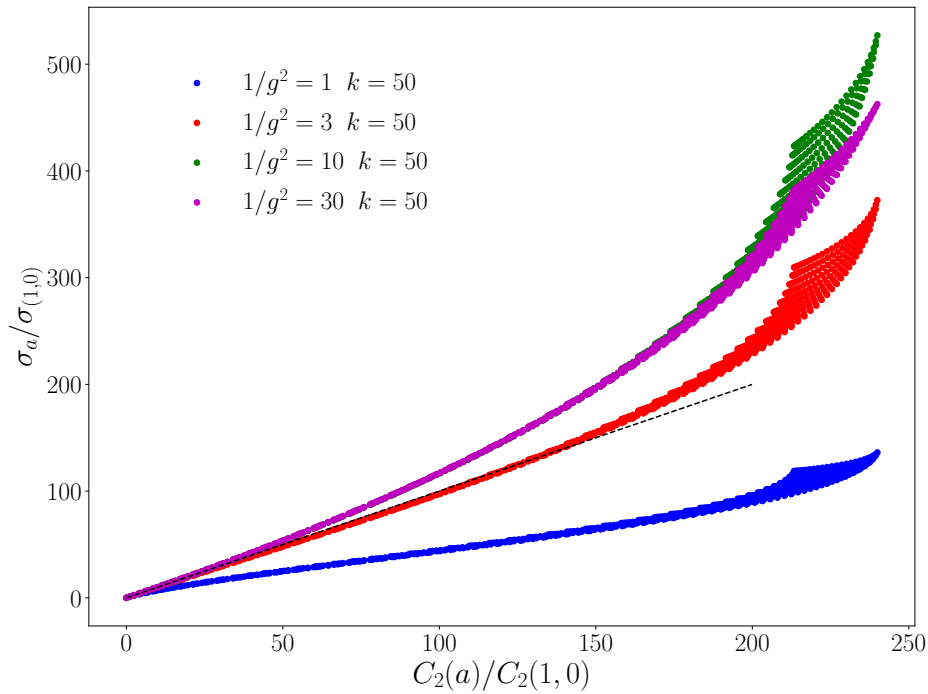


Figure 6. String tension of the Wilson loop of various representations as a function of the Casimir invariant with $k = 50$, and $1/g^2 = 1, 3, 10, 30$. The black dashed line shows the Casimir scaling $\sigma_a/\sigma_{(1,0)} = C_2(a)/C_2(1,0)$.

mean-field computation based on iPEPS indicates that the essential features of Yang-Mills theory can be captured by using tensor networks, so that tensor networks would be useful for future studies of Yang-Mills theory and QCD.

Even within the mean-field approximation, we have several directions to improve the analysis. First, it is important to compute other observables such as the mass of glueballs. We can compute the imaginary-time correlation function of Wilson loops with the present mean-field computation, from which we may read off the lightest glueball mass as is commonly done in the conventional lattice simulations. Second, we need to generalize the computation to $(3+1)$ dimensions and incorporate fermions for studying QCD. It would also be important to study the nonequilibrium physics such as thermalization [59]. We can study nonequilibrium dynamics by changing the imaginary-time evolution (4.23) to the real-time evolution, and making variational parameters spatially inhomogeneous. Such an analysis may correspond to the time-dependent mean field approximation. We will address these problems in future works.

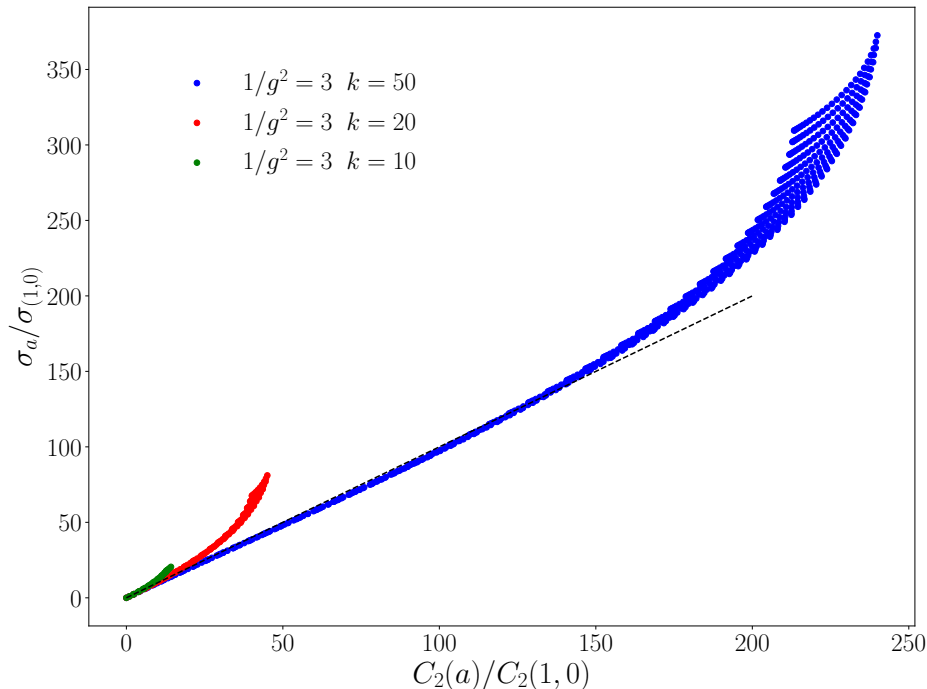


Figure 7. String tension of the Wilson loop of various representations as a function of the Casimir invariant with $k = 10, 20, 50$, and $1/g^2 = 3$. The black dashed line shows the Casimir scaling $\sigma_a/\sigma_{(1,0)} = C_2(a)/C_2(1,0)$.

Acknowledgements

The numerical calculations were carried out on cluster computers at iTHEMS in RIKEN. This work was supported by JSPS KAKENHI Grant Numbers 21H01007, and 21H01084.

Bibliography

- [1] F. Gross et al., *50 Years of Quantum Chromodynamics*, [2212.11107](#).
- [2] P. de Forcrand, *Simulating QCD at finite density*, *PoS LAT2009* (2009) 010 [[1005.0539](#)].
- [3] G. Aarts, *Introductory lectures on lattice QCD at nonzero baryon number*, *J. Phys. Conf. Ser.* **706** (2016) 022004 [[1512.05145](#)].
- [4] A. Alexandru, G. Basar, P.F. Bedaque and N.C. Warrington, *Complex paths around the sign problem*, *Rev. Mod. Phys.* **94** (2022) 015006 [[2007.05436](#)].
- [5] K. Nagata, *Finite-density lattice QCD and sign problem: Current status and open problems*, *Prog. Part. Nucl. Phys.* **127** (2022) 103991 [[2108.12423](#)].
- [6] J.I. Cirac and P. Zoller, *Goals and opportunities in quantum simulation*, *Nature Physics* **8** (2012) 264.

- [7] I.M. Georgescu, S. Ashhab and F. Nori, *Quantum Simulation*, *Rev. Mod. Phys.* **86** (2014) 153 [[1308.6253](#)].
- [8] R. Orus, *A Practical Introduction to Tensor Networks: Matrix Product States and Projected Entangled Pair States*, *Annals Phys.* **349** (2014) 117 [[1306.2164](#)].
- [9] J.I. Cirac, D. Perez-Garcia, N. Schuch and F. Verstraete, *Matrix product states and projected entangled pair states: Concepts, symmetries, theorems*, *Rev. Mod. Phys.* **93** (2021) 045003 [[2011.12127](#)].
- [10] M. Dalmonte and S. Montangero, *Lattice gauge theory simulations in the quantum information era*, *Contemp. Phys.* **57** (2016) 388 [[1602.03776](#)].
- [11] J. Preskill, *Simulating quantum field theory with a quantum computer*, *PoS LATTICE2018* (2018) 024 [[1811.10085](#)].
- [12] M.C. Bañuls and K. Cichy, *Review on Novel Methods for Lattice Gauge Theories*, *Rept. Prog. Phys.* **83** (2020) 024401 [[1910.00257](#)].
- [13] M.C. Bañuls et al., *Simulating Lattice Gauge Theories within Quantum Technologies*, *Eur. Phys. J. D* **74** (2020) 165 [[1911.00003](#)].
- [14] E. Zohar, *Quantum simulation of lattice gauge theories in more than one space dimension—requirements, challenges and methods*, *Phil. Trans. A. Math. Phys. Eng. Sci.* **380** (2021) 20210069 [[2106.04609](#)].
- [15] R. Anishetty and T.P. Sreeraj, *Mass gap in the weak coupling limit of (2+1)-dimensional $SU(2)$ lattice gauge theory*, *Phys. Rev. D* **97** (2018) 074511 [[1802.06198](#)].
- [16] I. Raychowdhury, *Low energy spectrum of $SU(2)$ lattice gauge theory: An alternate proposal via loop formulation*, *Eur. Phys. J. C* **79** (2019) 235 [[1804.01304](#)].
- [17] N. Klco, J.R. Stryker and M.J. Savage, *$SU(2)$ non-Abelian gauge field theory in one dimension on digital quantum computers*, *Phys. Rev. D* **101** (2020) 074512 [[1908.06935](#)].
- [18] I. Raychowdhury and J.R. Stryker, *Loop, string, and hadron dynamics in $SU(2)$ Hamiltonian lattice gauge theories*, *Phys. Rev. D* **101** (2020) 114502 [[1912.06133](#)].
- [19] W.J. Cunningham, B. Dittrich and S. Steinhaus, *Tensor Network Renormalization with Fusion Charges—Applications to 3D Lattice Gauge Theory*, *Universe* **6** (2020) 97 [[2002.10472](#)].
- [20] S. A Rahman, R. Lewis, E. Mendicelli and S. Powell, *$SU(2)$ lattice gauge theory on a quantum annealer*, *Phys. Rev. D* **104** (2021) 034501 [[2103.08661](#)].
- [21] T. Hayata, Y. Hidaka and Y. Kikuchi, *Diagnosis of information scrambling from Hamiltonian evolution under decoherence*, *Phys. Rev. D* **104** (2021) 074518 [[2103.05179](#)].
- [22] D. González-Cuadra, T.V. Zache, J. Carrasco, B. Kraus and P. Zoller, *Hardware Efficient Quantum Simulation of Non-Abelian Gauge Theories with Qudits on Rydberg Platforms*, *Phys. Rev. Lett.* **129** (2022) 160501 [[2203.15541](#)].
- [23] X. Yao, *$SU(2)$ Non-Abelian Gauge Theory on a Plaquette Chain Obeys Eigenstate Thermalization Hypothesis*, [2303.14264](#).
- [24] T.V. Zache, D. González-Cuadra and P. Zoller, *Quantum and classical spin network algorithms for q -deformed Kogut-Susskind gauge theories*, [2304.02527](#).

- [25] T. Hayata and Y. Hidaka, *String-net formulation of Hamiltonian lattice Yang-Mills theories and quantum many-body scars in a nonabelian gauge theory*, [2305.05950](#).
- [26] J.C. Halimeh, L. Homeier, A. Bohrdt and F. Grusdt, *Spin exchange-enabled quantum simulator for large-scale non-Abelian gauge theories*, [2305.06373](#).
- [27] T. Byrnes and Y. Yamamoto, *Simulating lattice gauge theories on a quantum computer*, *Phys. Rev. A* **73** (2006) 022328 [[quant-ph/0510027](#)].
- [28] A. Ciavarella, N. Klco and M.J. Savage, *Trailhead for quantum simulation of $SU(3)$ Yang-Mills lattice gauge theory in the local multiplet basis*, *Phys. Rev. D* **103** (2021) 094501 [[2101.10227](#)].
- [29] A.N. Ciavarella and I.A. Chernyshev, *Preparation of the $SU(3)$ lattice Yang-Mills vacuum with variational quantum methods*, *Phys. Rev. D* **105** (2022) 074504 [[2112.09083](#)].
- [30] J.B. Kogut and L. Susskind, *Hamiltonian Formulation of Wilson's Lattice Gauge Theories*, *Phys. Rev. D* **11** (1975) 395.
- [31] R. Penrose, *Angular momentum: an approach to combinatorial space-time*, *Quantum theory and beyond* **151** (1971) .
- [32] C. Rovelli and L. Smolin, *Spin networks and quantum gravity*, *Phys. Rev. D* **52** (1995) 5743 [[gr-qc/9505006](#)].
- [33] J.C. Baez, *Spin network states in gauge theory*, *Adv. Math.* **117** (1996) 253 [[gr-qc/9411007](#)].
- [34] G. Burgio, R. De Pietri, H.A. Morales-Tecotl, L.F. Urrutia and J.D. Vergara, *The Basis of the physical Hilbert space of lattice gauge theories*, *Nucl. Phys. B* **566** (2000) 547 [[hep-lat/9906036](#)].
- [35] B. Dittrich, *Cosmological constant from condensation of defect excitations*, *Universe* **4** (2018) 81 [[1802.09439](#)].
- [36] A. Kitaev, *Anyons in an exactly solved model and beyond*, *Annals Phys.* **321** (2006) 2 [[cond-mat/0506438](#)].
- [37] M. Barkeshli, P. Bonderson, M. Cheng and Z. Wang, *Symmetry Fractionalization, Defects, and Gauging of Topological Phases*, *Phys. Rev. B* **100** (2019) 115147 [[1410.4540](#)].
- [38] P. Bonderson, K. Shtengel and J.K. Slingerland, *Interferometry of non-Abelian Anyons*, *Annals Phys.* **323** (2008) 2709 [[0707.4206](#)].
- [39] L. Begin, P. Mathieu and M.A. Walton, *$SU(3)$ - k fusion coefficients*, *Mod. Phys. Lett. A* **7** (1992) 3255 [[hep-th/9206032](#)].
- [40] D. Bonatsos and C. Daskaloyannis, *Quantum groups and their applications in nuclear physics*, *Prog. Part. Nucl. Phys.* **43** (1999) 537 [[nucl-th/9909003](#)].
- [41] R. Coquereaux, D. Hammaoui, G. Schieber and E.H. Tahri, *Comments about quantum symmetries of $SU(3)$ graphs*, *J. Geom. Phys.* **57** (2006) 269 [[math-ph/0508002](#)].
- [42] E. Ardonne and J. Slingerland, *Clebsch-gordan and 6j-coefficients for rank 2 quantum groups*, *Journal of Physics A: Mathematical and Theoretical* **43** (2010) 395205 [[1004.5456](#)].
- [43] M.A. Levin and X.-G. Wen, *String net condensation: A Physical mechanism for topological phases*, *Phys. Rev. B* **71** (2005) 045110 [[cond-mat/0404617](#)].

- [44] S. Dusuel and J. Vidal, *Mean-field ansatz for topological phases with string tension*, *Phys. Rev. B* **92** (2015) 125150 [[1506.03259](#)].
- [45] A. Ritz-Zwilling, J.-N. Fuchs and J. Vidal, *Wegner-Wilson loops in string nets*, *Phys. Rev. B* **103** (2021) 075128 [[2011.12609](#)].
- [46] M. Ringbauer, M. Meth, L. Postler, R. Stricker, R. Blatt, P. Schindler et al., *A universal qudit quantum processor with trapped ions*, *Nature Phys.* **18** (2022) 1053 [[2109.06903](#)].
- [47] R. Koenig, G. Kuperberg and B.W. Reichardt, *Quantum computation with Turaev-Viro codes*, *Annals Phys.* **325** (2010) 2707 [[1002.2816](#)].
- [48] A. Schotte, G. Zhu, L. Burgelman and F. Verstraete, *Quantum Error Correction Thresholds for the Universal Fibonacci Turaev-Viro Code*, *Phys. Rev. X* **12** (2022) 021012 [[2012.04610](#)].
- [49] P. Bialas, L. Daniel, A. Morel and B. Petersson, *Thermodynamics of $SU(3)$ Gauge Theory in $2 + 1$ Dimensions*, *Nucl. Phys. B* **807** (2009) 547 [[0807.0855](#)].
- [50] L. Vanderstraeten, M. Mariën, J. Haegeman, N. Schuch, J. Vidal and F. Verstraete, *Bridging perturbative expansions with tensor networks*, *Phys. Rev. Lett.* **119** (2017) 070401.
- [51] A. Schotte, J. Carrasco, B. Vanhecke, J. Haegeman, L. Vanderstraeten, F. Verstraete et al., *Tensor-network approach to phase transitions in string-net models*, *Phys. Rev. B* **100** (2019) 245125 [[1909.06284](#)].
- [52] J. Ambjorn, P. Olesen and C. Peterson, *Stochastic Confinement and Dimensional Reduction. 1. Four-Dimensional $SU(2)$ Lattice Gauge Theory*, *Nucl. Phys. B* **240** (1984) 189.
- [53] J. Ambjorn, P. Olesen and C. Peterson, *Stochastic Confinement and Dimensional Reduction. 2. Three-dimensional $SU(2)$ Lattice Gauge Theory*, *Nucl. Phys. B* **240** (1984) 533.
- [54] S. Deldar, *Static $SU(3)$ potentials for sources in various representations*, *Phys. Rev. D* **62** (2000) 034509 [[hep-lat/9911008](#)].
- [55] G.S. Bali, *Casimir scaling of $SU(3)$ static potentials*, *Phys. Rev. D* **62** (2000) 114503 [[hep-lat/0006022](#)].
- [56] Z.-C. Gu, M. Levin, B. Swingle and X.-G. Wen, *Tensor-product representations for string-net condensed states*, *Phys. Rev. B* **79** (2009) 085118.
- [57] O. Buerschaper, M. Aguado and G. Vidal, *Explicit tensor network representation for the ground states of string-net models*, *Phys. Rev. B* **79** (2009) 085119.
- [58] T. Soejima, K. Siva, N. Bultinck, S. Chatterjee, F. Pollmann and M.P. Zaletel, *Isometric tensor network representation of string-net liquids*, *Phys. Rev. B* **101** (2020) 085117.
- [59] T. Hayata and Y. Hidaka, *Thermalization of Yang-Mills theory in a $(3 + 1)$ dimensional small lattice system*, *Phys. Rev. D* **103** (2021) 094502 [[2011.09814](#)].